
HOKKAIDO UNIVERSITY

Title	Repulsion and absorption of the Σ-nucleus potential for Σ−−5He in the 6Li(π−,K+) reaction
Author(s)	Harada, Toru; Honda, Ryotaro; Hirabayashi, Yoshiharu
Citation	Physical Review C, 97(2), 024601 https://doi.org/10.1103/PhysRevC.97.024601
Issue Date	2018-02-01
Doc URL	http://hdl.handle.net/2115/68585
Rights	©2018 American Physical Society
Type	article
File Information	PhysRevC.97.024601-1.pdf


Instructions for use

Hokkaido University Collection of Scholarly and Academic Papers : HUSCAP

Repulsion and absorption of the Σ-nucleus potential for Σ^--^{5}He in the ^{6}Li(π^-, K^+) reaction

Toru Harada,[1,2,*] Ryotaro Honda,[3] and Yoshiharu Hirabayashi[4]

[1]*Research Center for Physics and Mathematics, Osaka Electro-Communication University, Neyagawa, Osaka, 572-8530, Japan*

[2]*J-PARC Branch, KEK Theory Center, Institute of Particle and Nuclear Studies, High Energy Accelerator Research Organization (KEK), 203-1, Shirakata, Tokai, Ibaraki, 319-1106, Japan*

[3]*Department of Physics, Tohoku University, Sendai, Miyagi, 980-8578, Japan*

[4]*Information Initiative Center, Hokkaido University, Sapporo, 060-0811, Japan*

(Received 19 July 2017; revised manuscript received 2 October 2017; published 1 February 2018)

We study phenomenologically inclusive spectra of the ^{6}Li(π^-, K^+) reaction at 1.2 GeV/c within a distorted-wave impulse approximation with the optimal Fermi-averaging $\pi^- p \to K^+ \Sigma^- t$ matrix. We attempt to clarify the property of a Σ-nucleus potential for Σ^--^{5}He by comparing the calculated spectra with the data of the J-PARC E10 experiment. The result shows that the repulsive and absorptive components of the Σ^--^{5}He potential provide the ability to explain the data of the continuum spectra in Σ and Λ regions; the strengths of $V_\Sigma = +30 \pm 10$ MeV and $W_\Sigma = -26 \pm 2$ MeV are favored within the Woods-Saxon potential, consistent with analyses for heavier nuclei. Effects of the size and potential range for Σ^--^{5}He in the neutron excess of $(N - Z)/(N + Z) = 0.2$ are also discussed.

DOI: 10.1103/PhysRevC.97.024601

I. INTRODUCTION

Recently, the J-PARC E10 Collaboration [1,2] performed experimental measurements of the double charge-exchange (DCX) reaction (π^-, K^+) on a ^{6}Li target at $p_{\pi^-} = 1.2$ GeV/c; missing mass spectra from Λ to Σ regions were obtained with K^+ forward-direction angles of $\theta_{\rm lab} = 2^\circ$–$14^\circ$, whereas no significant peak structure of a neutron-rich $^6_\Lambda$H hypernucleus was observed around the $^4_\Lambda$H + $2n$ threshold [1,2]. This reaction can also populate $\Sigma^- \otimes {}^5$He doorway states with $T = 3/2$ in a $^6_\Sigma$H hypernucleus by a $\pi^- p \to K^+ \Sigma^-$ process in the nuclear medium [3]. One expects that a Σ-nucleus potential for Σ^--^{5}He can be studied by comparing a theoretical calculation with the data of the missing mass spectra at $\theta_{\rm lab} = 2^\circ$–$14^\circ$ in the reaction [2].

The DCX (π^-, K^+) reactions on nuclear targets provide investigation for the Σ-nucleus potential analyzing quasifree (QF) Σ^- production spectra. Noumi and his collaborators [4,5] performed measurements of Σ-hypernuclei by inclusive (π^-, K^+) reactions on heavier targets at $p_{\pi^-} = 1.2$ GeV/c in the KEK-E438 experiment. Their analysis within a distorted-wave impulse approximation (DWIA) indicated that the Σ-nucleus potential has a strong repulsion in the real part and a sizable absorption in the imaginary part [5]. Batty and his collaborators [6,7] studied the Σ-nucleus potential analyzing Σ^- atomic x-ray data systematically. Thus the latest studies [6–11] have suggested that the Σ-nucleus potential has a repulsion inside the nuclear surface and a shallow attraction outside the nucleus with a sizable absorption, e.g., the density-dependent (DD) potential [6]. This repulsion may originate from ΣN $I = 3/2$, $^3S_1$ channel [12–14], whose state corresponds to a quark Pauli-forbidden state in a baryon-baryon system [15], as supported by modern YN potentials [16] and also recent lattice QCD calculations [17].

Harada and Hirabayashi [10,11] succeeded in explaining the data of the (π^-, K^+) reaction at 1.2 GeV/c on ^{28}Si and ^{209}Bi targets, performing DWIA calculations with the optimal Fermi averaging for the $\pi^- p \to K^+ \Sigma^-$ reaction. Their analysis with the DWIA [10,11] also suggested that the Σ-nucleus potential within the Woods-Saxon (WS) or 2pF form is

$$U_\Sigma(r) = (V_\Sigma + i W_\Sigma)/\{1 + \exp[(r - R)/a]\} \qquad (1)$$

with $R = 1.1 A_{\rm core}^{1/3}$ and $a = 0.67$ fm, where $V_\Sigma = (+20)$–$(+30)$ MeV and $W_\Sigma = (-20)$–(-40) MeV, corresponding to a strong repulsion in the real part and a sizable absorption in the imaginary part of the potential. It is very important to study a negatively charged Σ^- hyperon in the nuclear medium in order to obtain valuable information concerning the maximal mass of neutron stars, in which a baryon fraction is found to depend on properties of the Σ^- potentials for astrophysics [18]. The Σ-nucleus interaction may be established as being repulsive so far, but it is still an open problem how repulsive the Σ-nucleus potential is [19,20].

In this paper, we investigate phenomenologically the inclusive spectra of Σ hypernuclear production by the ^{6}Li(π^-, K^+) reaction at 1.2 GeV/c in order to extract valuable information on the Σ-nucleus (optical) potential for Σ^--^{5}He from the data of the J-PARC E10 experiment [2]. We demonstrate the calculated spectra within the DWIA, using the optimal Fermi-averaging t matrix for the $\pi^- p \to K^+ \Sigma^-$ reaction in the nuclear medium because the energy dependence of the t matrix is important to explain the behavior of the (π^-, K^+) spectrum [10]. By using a single-particle $\Sigma^- \otimes {}^5$He model with a spreading potential, we study the nature of the repulsion and absorption in the Σ-nucleus potential, in comparison with the data of the J-PARC E10 experiment.

*harada@osakac.ac.jp

 ©2018 American Physical Society

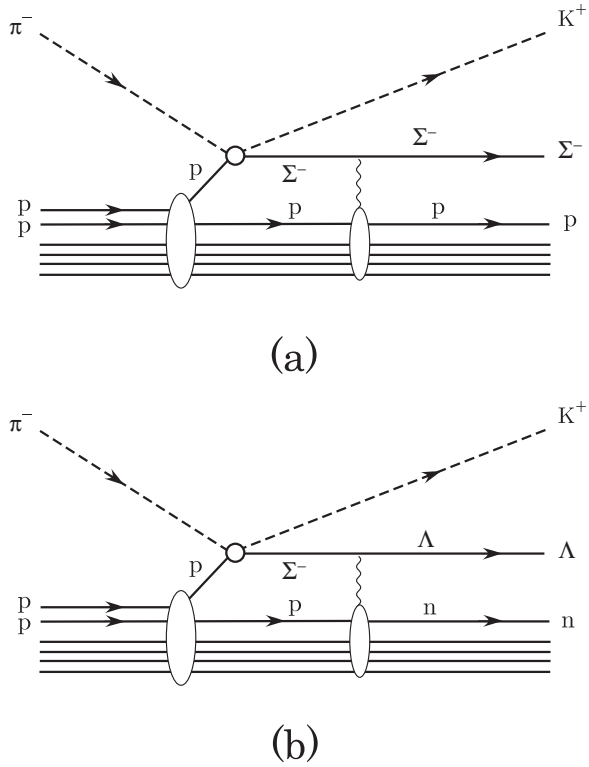

FIG. 1. Diagrams for double-charge exchange (π^-, K^+) reactions on nuclear targets, leading to production of (a) Σ hypernuclear states by $\pi^- p \to K^+\Sigma^-$ processes and (b) Λ hypernuclear states caused by the $\Sigma^- p \leftrightarrow \Lambda n$ coupling.

II. CALCULATIONS

A. Distorted wave impulse approximation

Let us consider production of Σ hypernuclear states in the DCX reaction (π^-, K^+) on a nuclear target. Figure 1 illustrates diagrams for the nuclear (π^-, K^+) reaction by $\pi^- p \to K^+\Sigma^-$ processes for the Σ hypernuclear states, and by $\pi^- p \to K^+\Sigma^-$ via Σ^- doorways caused by the $\Sigma^- p \to \Lambda n$ conversion for Λ hypernuclear excited states. According to the Green's function method [21] in the DWIA, an inclusive K^+ double-differential laboratory cross section of the Σ production on the nuclear target with a spin J_A (its z component M_A) [22] is given by

$$\frac{d^2\sigma}{d\Omega dE} = \frac{1}{[J_A]} \sum_{M_A} S(E) \tag{2}$$

with $[J_A] = 2J_A + 1$. The strength function $S(E)$ is written as

$$S(E) = -\frac{1}{\pi} \mathrm{Im} \sum_{\alpha\alpha'} \int d\boldsymbol{r} d\boldsymbol{r}' F_\Sigma^{\alpha\,\dagger}(\boldsymbol{r}) G_\Sigma^{\alpha\alpha'}(E;\boldsymbol{r},\boldsymbol{r}') F_\Sigma^{\alpha'}(\boldsymbol{r}'), \tag{3}$$

where $G_\Sigma^{\alpha\alpha'}$ is a complete Green's function, F_Σ^α is a Σ production amplitude defined by

$$F_\Sigma^\alpha = \beta^{\frac{1}{2}} \overline{f}_{\pi^- p \to K^+\Sigma^-} \chi_{\boldsymbol{p}_K}^{(-)*} \chi_{\boldsymbol{p}_\pi}^{(+)} \langle \alpha \,|\hat{\psi}_p|\, \Psi_A \rangle, \tag{4}$$

and $\langle \alpha \,|\hat{\psi}_p|\, \Psi_A \rangle$ is a hole-state wave function for a struck proton in the target; α (α') denotes the complete set of eigenstates for the system. The laboratory energy and momentum transfer is

$$\omega = E_K - E_\pi, \qquad \boldsymbol{q} = \boldsymbol{p}_K - \boldsymbol{p}_\pi, \tag{5}$$

where E_K and $\boldsymbol{p}_K$ (E_π and $\boldsymbol{p}_\pi$) denote the energy and momentum of the outgoing K^+ (the incoming π^-), respectively. The kinematical factor β denotes the translation from the two-body π^--p laboratory system to the π^--^{6}Li laboratory system. $\overline{f}_{\pi^- p \to K^+\Sigma^-}$ is a Fermi-averaged amplitude for the $\pi^- p \to K^+\Sigma^-$ reaction in the nuclear medium [10,11,23]. $\chi_{\boldsymbol{p}_K}^{(-)}$ and $\chi_{\boldsymbol{p}_\pi}^{(+)}$ are distorted waves for the outgoing K^+ and incoming π^- mesons, respectively.

B. ^{6}Li target

For the ^{6}Li target, we assume single-particle (s.p.) description of a proton for simplicity [24], although the state of $^6\mathrm{Li}(1^+_{\mathrm{g.s.}}; T = 0)$ is well described as $\alpha + d$ clusters [25]. Thus, a s.p. wave function for the proton in $0p_{3/2}$ ($0s_{1/2}$) is calculated by the WS potential with $a = 0.67$ fm, $R = 1.27A^{1/3} = 2.31$ fm [26]. The strength parameter of the potential must be adjusted to be $V_0^N = -55.5$ MeV (-58.0 MeV) for the proton in the $p_{3/2}$ ($s_{1/2}$) state, and $V_{\mathrm{so}}^N = -0.44V_0^N$, in order to reproduce the data of proton s.p. energies in $^6\mathrm{Li}(p,2p)$ reactions [27,28]. Thus we obtain the s.p. energies of -4.61 MeV for $0p_{3/2}$ and -21.48 MeV for $0s_{1/2}$, and the charge radius for $^6\mathrm{Li}(1^+_{\mathrm{g.s.}})$ becomes 2.48 fm. This value in the s.p. model is slightly smaller than that of 2.56 ± 0.05 fm in electron elastic scatterings [29] because the structure of $\alpha + d$ clusters is not taken into account [25].

C. Eikonal distortion

Due to a high momentum transfer $q \simeq 320$–600 MeV/c in the (π^-, K^+) reaction at K^+ forward-direction angles of $\theta_{\mathrm{lab}} = 2^\circ$–$14^\circ$, we simplify the computational procedure for the distorted waves, $\chi_{\boldsymbol{p}_K}^{(-)}$ and $\chi_{\boldsymbol{p}_\pi}^{(+)}$, using the eikonal approximation. To reduce ambiguities in the distorted waves, we adopt the same parameters used in calculations for the Λ and Σ^- QF spectra in nuclear $(\pi^\mp, K^+)$ reactions [10,11,23]. Here we used total cross sections of $\sigma_\pi = 32$ mb for $\pi^- N$ scattering and $\sigma_K = 12$ mb for $K^+ N$ one, and $\alpha_\pi = \alpha_K = 0$, as the distortion parameters. We took into account the recoil effects because the effects are very important to estimate the production spectra for the light nuclear system, leading to an effective momentum transfer having $q_{\mathrm{eff}} \simeq (1 - 1/A)q \simeq 0.83q$ for $A = 6$.

D. Green's functions

To calculate the nuclear (π^-, K^+) spectra in the DWIA, we employ the Green's function method [21], which is one of the most powerful treatments in the calculation of a spectrum in which not only bound states but also continuum states are described with an absorptive potential for spreading components. The complete Green's function $G(E)$ has all information concerning $\Sigma^- \otimes {}^5$He dynamics, and it can be obtained by

solving the following equation numerically:

$$G_\Sigma(E) = G_\Sigma^{(0)}(E) + G_\Sigma^{(0)}(E)U_\Sigma(E)G_\Sigma(E), \tag{6}$$

where $G_\Sigma^{(0)}$ is the free Green's function. The Σ-nucleus (optical) potential is given by

$$U_\Sigma(E) = PUP + PUQG(E+i\epsilon)QUP, \tag{7}$$

where U is the hyperon-nucleus interaction and $P+Q=1$ in the Feshbach projection method. The strength function $S(E)$ in Eq. (3) can be evaluated by taking the complete Green's function G_Σ in Eq. (6), which fully includes Σ^- doorways by $\pi^- p \to K^+\Sigma^-$ reactions [30], as shown in Fig. 1. Because non-spin-flip processes seem to dominate in $\pi^- p \to K^+\Sigma^-$ reactions at 1.2 GeV/c [31], configurations of $\Sigma^- \otimes {}^5$He with $T = 3/2, J^\pi = (1^+ \otimes \Delta L) = 1^+, 0^-, 1^-, 2^-, 1^+, 2^+, 3^+, \ldots$, can be populated where $\Delta L = 0, 1, 2, \ldots$, denote the angular momentum transfer to ${}^6\mathrm{Li}(1^+_{\mathrm{g.s.}})$. No Λ channel is explicitly taken into account because the ΣΛ coupling effects may be described as a spreading imaginary potential in continuum spectra in Σ regions.

III. OPTIMAL FERMI AVERAGING

As discussed in Refs. [10,11], the DWIA analyses of the Σ^- QF spectra in the nuclear (π^-, K^+) reactions indicated the importance of an energy dependence of the Fermi-averaged amplitude $\overline{f}_{\pi^- p\to K^+\Sigma^-}$ in order to extract properties of the potential from the data. In this version of the DWIA, the Fermi-averaged amplitude $\overline{f}_{\pi^- p\to K^+\Sigma^-}$ in Eq. (4) plays an important role in explaining a spectral shape in the nuclear (π^-, K^+) reaction [10,11]. We should use the $\pi^- p \to K^+\Sigma^- t$ matrix, which can fully reproduce the experimental data of differential cross sections in free space so as to obtain a suitable Fermi-averaged amplitude in our calculations. Thus we perform the optimal Fermi averaging for elementary $\pi^- p \to K^+\Sigma^-$ processes at each θ_{lab} in the nucleus [10,11].

A. $\pi^- p \to K^+\Sigma^-$ reactions

Very recently, new data of four angular points for the $\pi^- p \to K^+\Sigma^-$ reactions have been measured with excellent quality at $E_{\mathrm{c.m.}} = 1875$ MeV in the J-PARC E10 experiment [2]. Hence we improve the angular distributions of the differential cross section in the center-of-mass (c.m.) frame, whereas there is still no available amplitude of the $\pi^- p \to K^+\Sigma^-$ reaction due to poor quality in the other data [32]. The cross section is written as

$$\left(\frac{d\sigma}{d\Omega}\right)^{\mathrm{elem}}_{\mathrm{c.m.}} = \lambda\!\!\!^{-2} \sum_{\ell=0}^{\ell_{\max}} A_\ell(E_{\mathrm{c.m.}})P_\ell(\cos\theta_{\mathrm{c.m.}}) = \frac{\omega_f \omega_i p_f}{(2\pi)^2 p_i}|t_{\mathrm{c.m.}}(E_{\mathrm{c.m.}})|^2, \tag{8}$$

where $\lambda\!\!\!^{-}$ is the de Broglie wavelength of $\pi^- p$, and $P_\ell(x)$ are Legendre polynomials. Coefficient parameters $A_\ell(E_{\mathrm{c.m.}})$ are expressed by a power series of $E_{\mathrm{c.m.}}$ so as to make a fit to their energy dependence. $t_{\mathrm{c.m.}}(E_{\mathrm{c.m.}})$ denotes the elementary $\pi^- p \to K^+\Sigma^- t$ matrix in the c.m. frame, and p_f (p_i) and ω_f (ω_i) are a momentum and a reduced energy for $K^+\Sigma^-$ ($\pi^- p$) in the c.m. frame, respectively.

In Fig. 2, we show the angular distributions at various c.m. energies $E_{\mathrm{c.m.}}$, together with the data [2,32]. The angular distributions near $E_{\mathrm{c.m.}} = 1875$ MeV are improved for fits to the data newly observed in the J-PARC E10 experiment [2], whereas the value of an integrated cross section $\sigma^{\mathrm{tot}}_{\mathrm{c.m.}}(E_{\mathrm{c.m.}})$ is not so changed from that of the previous one [10,11].

B. Optimal Fermi-averaged t matrix

To fully describe the energy dependence of the (π^-, K^+) reaction on a target nucleus, which comes from N^* resonances in the $\pi^- p \to K^+\Sigma^-$ processes, we must adopt the optimal Fermi averaging [23] for the $\pi^- p \to K^+\Sigma^-$ reaction in the nucleus. In this version of the DWIA, an optimal cross section for the elementary $\pi^- p \to K^+\Sigma^-$ processes in the nucleus [10] can be given as

$$\left(\frac{d\sigma}{d\Omega}\right)^{\mathrm{opt}} \equiv \beta|\overline{f}_{\pi^- p\to K^+\Sigma^-}|^2 = \frac{p_K E_K}{(2\pi)^2 v_\pi}\left|t^{\mathrm{opt}}_{\pi N,K\Sigma}(p_\pi;\omega,\boldsymbol{q})\right|^2, \tag{9}$$

where $v_\pi = p_\pi/E_\pi$, and $t^{\mathrm{opt}}_{\pi N,K\Sigma}(p_\pi;\omega,\boldsymbol{q})$ is an optimal Fermi-averaged $\pi^- p \to K^+\Sigma^- t$ matrix, which is defined by

$$t^{\mathrm{opt}}_{\pi N,K\Sigma}(p_\pi;\omega,\boldsymbol{q}) = \left.\frac{\int_0^\pi \sin\theta_N d\theta_N \int_0^\infty dp_N\, p_N^2 \rho(p_N) t_{\pi N,K\Sigma}(E_2;\boldsymbol{p}_\pi,\boldsymbol{p}_N)}{\int_0^\pi \sin\theta_N d\theta_N \int_0^\infty dp_N\, p_N^2 \rho(p_N)}\right|_{\boldsymbol{p}_N=\boldsymbol{p}^*_N}, \tag{10}$$

where E_N and $\boldsymbol{p}_N$ are the energy and momentum of a proton in the target nucleus, respectively; $\cos\theta_N = \hat{\boldsymbol{p}}_\pi \cdot \hat{\boldsymbol{p}}_N$, $E_2 = E_\pi + E_N$ is a total energy of the πN system, and $\rho(p_N)$ is a Fermi-momentum distribution of the proton in the target nucleus. The momentum $\boldsymbol{p}^*_N$ in Eq. (10) is a solution, which satisfies the on-energy-shell equation for a struck proton in the nuclear systems,

$$\sqrt{(\boldsymbol{p}^*_N + \boldsymbol{q})^2 + m_\Sigma^2} - \sqrt{(\boldsymbol{p}^*_N)^2 + m_N^2} = \omega, \tag{11}$$

where m_Σ and m_N are masses of the Σ^- and the proton, respectively. This procedure constructed from the on-energy-shell $\pi^- p \to K^+\Sigma^-$ processes in the nucleus [33] guarantees to have optimal values for $\overline{f}_{\pi^- p\to K^+\Sigma^-}$ in a factorized form of Eq. (4). Here we neglected the energy dependence of a phase in the $\pi^- p \to K^+\Sigma^- t$ matrix, and replaced $t_{\pi N,K\Sigma}(E_2;\boldsymbol{p}_\pi,\boldsymbol{p}_N)$ in the laboratory frame by its absolute value $|t_{\pi N,K\Sigma}(E_2;\boldsymbol{p}_\pi,\boldsymbol{p}_N)|$, which is obtained from the corresponding one in the c.m. frame in Eq. (8);

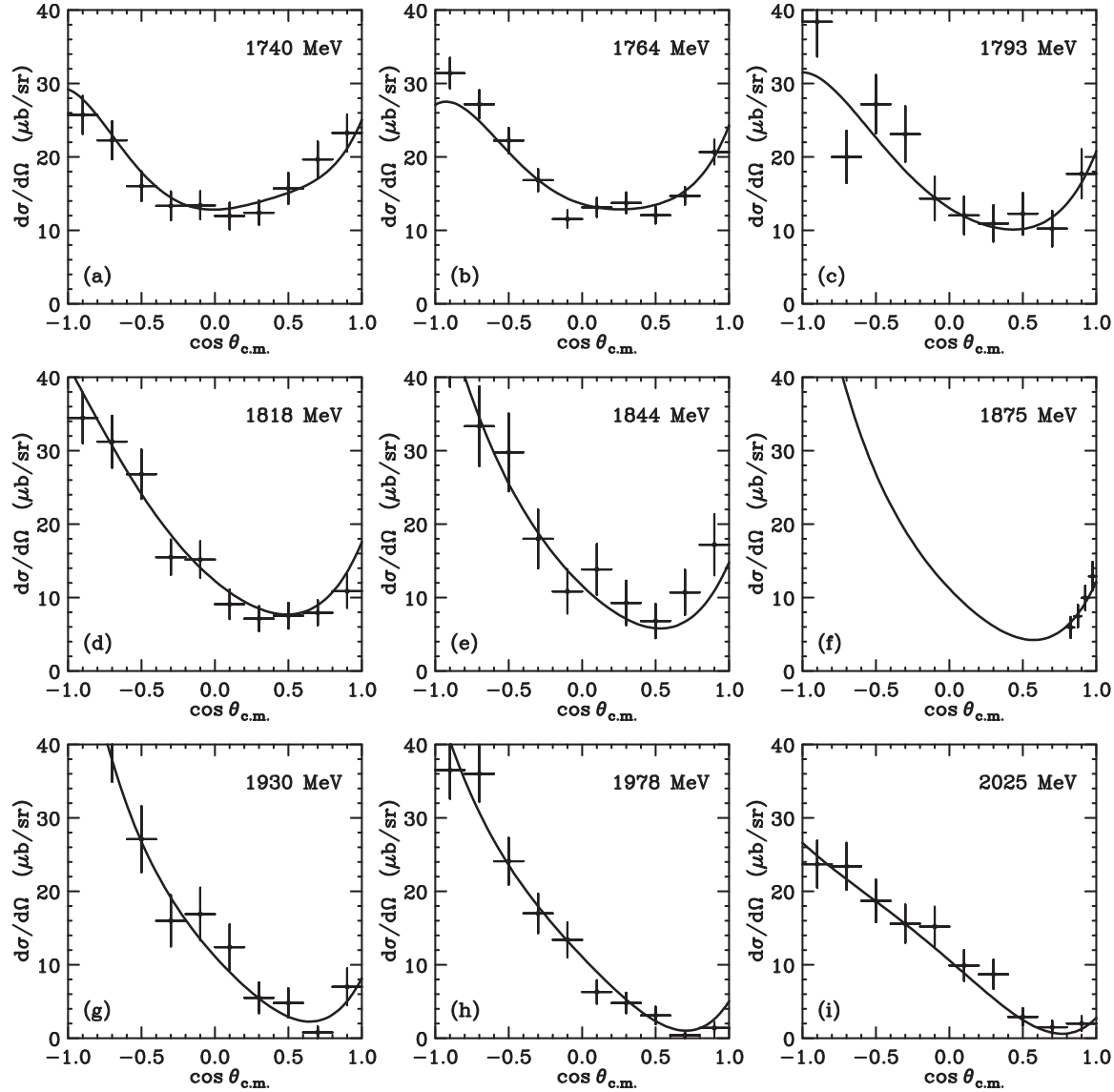

FIG. 2. Calculated angular distributions of the differential cross section for the $\pi^- p \to K^+\Sigma^-$ reaction in the c.m. frame at $E_{\rm c.m.} = 1740$, 1764, 1793, 1818, 1844, 1875, 1930, 1978, and 2025 MeV, together with the data [2,32].

$t_{\pi N,K\Sigma}(E_2; \boldsymbol{p}_\pi, \boldsymbol{p}_N) = \eta\, t_{\rm c.m.}(E_{\rm c.m.})$, where η is the Möller factor. Such an assumption has been confirmed to be appropriate in the case of the $\pi^+ n \to K^+\Lambda$ reaction [23], leading to the ω dependence of $(d\sigma/d\Omega)^{\rm opt}$, which is significant to describe the behavior of the $(\pi^\pm, K^+)$ reactions [10].

In Fig. 3, we show the optimal Fermi-averaged cross sections of $(d\sigma/d\Omega)^{\rm opt}$ at $\theta_{\rm lab} = 3^\circ$, 5°, 7°, 9°, 11°, and 13° in the region from Λ to Σ^-. We confirm that there appears a strong energy dependence of the $\pi^- p \to K^+\Sigma^-$ reaction in the nuclear medium, together with the angular dependence of $\theta_{\rm lab}$. Therefore, such behavior of $(d\sigma/d\Omega)^{\rm opt}$ would play a significant role in explaining the shape of the spectrum in the nuclear (π^-, K^+) reaction, as discussed in Refs. [10,11]. Because $\overline{f}_{\pi^- p \to K^+\Sigma^-}$ directly affects the spectral shape including widely the Σ^- QF region, thus one should carefully extract information concerning the Σ-nucleus potential from the data.

IV. Σ-NUCLEUS POTENTIAL

The Σ-nuclear final states are obtained by solving the Schrödinger equation

$$\left[-\frac{\hbar^2}{2\mu}\nabla^2 + U_\Sigma(r) + U_{\rm Coul}(r)\right]\Psi_\Sigma = E\Psi_\Sigma, \qquad (12)$$

where μ is the Σ-nucleus reduced mass, U_Σ is the Σ-nucleus potential, and $U_{\rm Coul}$ is the Coulomb potential. Here the Σ-nucleus potential for Σ^--^{5}He is given as

$$U_\Sigma(r) = [V_\Sigma + iW_\Sigma g(E_\Lambda)]f(r) \qquad (13)$$

with the assumption of the WS form

$$f(r) = \{1 + \exp[(r - R)/a]\}^{-1}, \qquad (14)$$

where $R = r_0 A_{\rm core}^{1/3}$ and a denote the radius and diffuseness of the potential, respectively, in order to be compared with the

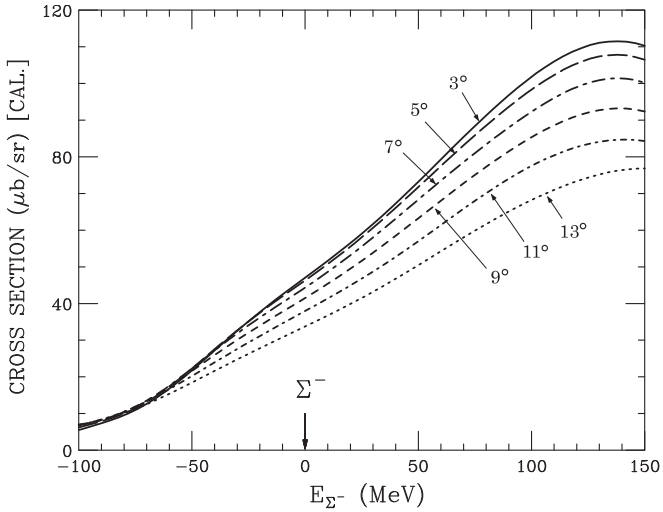

FIG. 3. Energy dependence of the optimal cross section $(d\sigma/d\Omega)^{\rm opt}$ for the $\pi^- p \to K^+\Sigma^-$ reaction on the ^{6}Li target at $p_{\pi^-} = 1.2$ GeV/c and $\theta_{\rm lab} = 3^\circ, 5^\circ, 7^\circ, 9^\circ, 11^\circ$, and 13°, as a function of E_{Σ^-}. The arrow shows the ^{5}He + Σ^- threshold.

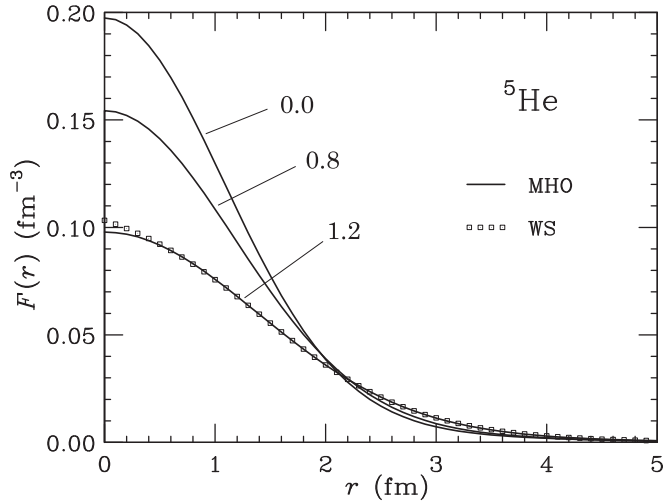

FIG. 4. Radial distributions of the form factors with Gaussian ranges of 0.0, 0.80, and 1.20 fm for the ^{5}He$(3/2^-_{\rm g.s.})$ nucleus, as a function of the radial distance. Solid curves and square symbols denote the distributions with the modified harmonic oscillator (MHO) and the Woods-Saxon (WS) models, respectively.

Σ-nucleus potentials for Σ^--^{27}Al [10] and Σ^--^{208}Pb [11]; $g(E_\Lambda)$ is an energy-dependent function, which linearly increases from 0.0 at $E_\Lambda = 0$ MeV to 1.0 at $E_\Lambda = 60$ MeV with respect to the Λ emitted threshold, as often used in nuclear optical models. The ground state of ^{5}He as the nuclear core is known to be a $3/2^-$ resonant state with the width of $\Gamma = 0.65$ MeV at the energy of $E_r = 0.80$ MeV with respect to the $\alpha + n$ threshold [27]. Thus the appropriate parameters of (r_0, a) for Eq. (14) must be used. For $U_{\rm Coul}$, we use an attractive Coulomb potential with the uniform distribution of a charged sphere where $Z = 2$ for Σ^--^{5}He.

A. Folding-model potential

To determine the parameters of (r_0, a) for the nuclear core in the WS form, we consider a folding-model potential obtained by convoluting the nuclear one-body density with a two-body $\Sigma^- N$ force [34]. The folding-model potential is given by

$$U_\Sigma(r) = \int v_{\Sigma N}(\boldsymbol{r} - \boldsymbol{r}')\rho(\boldsymbol{r}')d\boldsymbol{r}', \tag{15}$$

where $\rho(r)$ denotes the nuclear density distribution normalized by

$$4\pi \int_0^\infty \rho(r) r^2 dr = A_{\rm core}. \tag{16}$$

Because ^{5}He$(3/2^-_{\rm g.s.})$ is a p-wave resonant state with a narrow width ($\Gamma = 0.65$ MeV), the corresponding wave function may behave approximately as a bound-state one. Thus we assume the s.p. density of the shell model within bound-state approximation for simplicity; the modified harmonic oscillator (MHO) model is often used in the systematic description of the size and density distribution for He isotopes with $A = 4$, 6, and 8 [35]. We choose carefully the MHO size parameters of $b_s = 1.71$ fm and $b_p = 2.66$ fm for ^{5}He$(3/2^-_{\rm g.s.})$ with center-of-mass and nucleon-size corrections [36], providing the matter root-mean-square (rms) radius of $\langle r^2\rangle^{1/2} = 2.43$ fm, which is obtained by the $3/2^-$ resonant-state wave function calculated in the same procedure of Ref. [37]. For the two-body $\Sigma^- N$ force involving absorption, we assume a simple Gaussian form,

$$v_{\Sigma N}(r) = (\bar{v}_{\Sigma N} + i\bar{w}_{\Sigma N}) \exp\left(-r^2/a^2_{\Sigma N}\right), \tag{17}$$

where $\bar{v}_{\Sigma N}$ and $\bar{w}_{\Sigma N}$ are the real and imaginary parts of the ΣN spin-isospin averaged strength, respectively; the range of $a_{\Sigma N}$ is chosen to be 1.2 fm, consistent with the range of a hyperon-nucleon potential in free space [6], e.g., the D2′ potential [38]. We define a nuclear form factor as

$$F(r) = \int \rho_G(\boldsymbol{r} - \boldsymbol{r}')\rho(\boldsymbol{r}')d\boldsymbol{r}', \tag{18}$$

where $\rho_G(r) = (\sqrt{\pi}a_{\Sigma N})^{-3} \exp(-r^2/a^2_{\Sigma N})$, which is normalized as $4\pi \int \rho_G(r) r^2 dr = 1$. Thus we have

$$U_\Sigma(r) = (\bar{v}_{\Sigma N} + i\bar{w}_{\Sigma N})(\sqrt{\pi}a_{\Sigma N})^3 F(r), \tag{19}$$

where $4\pi \int F(r) r^2 dr = A_{\rm core}$. Figure 4 shows the form factors of $F(r)$ with $a_{\Sigma N} = 1.2, 0.8$, and 0.0 fm. For zero range ($a_{\Sigma N} = 0.0$ fm), $F(r)$ is equal to the matter MHO density distribution of ^{5}He$(3/2^-_{\rm g.s.})$. Note that $F(r)$ is reduced at the nuclear center because the radial distribution of the form factor is modified by $a_{\Sigma N}$ due to the small size of the nucleus.

B. Woods-Saxon parameters

For Σ^--^{5}He in the present work, we use the WS form with the parameters of (r_0, a) adjusted to give a best least-squares fit to the radial shape of the form factor obtained by folding a Gaussian range of $a_{\Sigma N} = 1.2$ fm into the matter MHO density distribution. The parameters of the resulting WS form in Eq. (14) are

$$r_0 = 0.835 \text{ fm}, \quad a = 0.706 \text{ fm}, \tag{20}$$

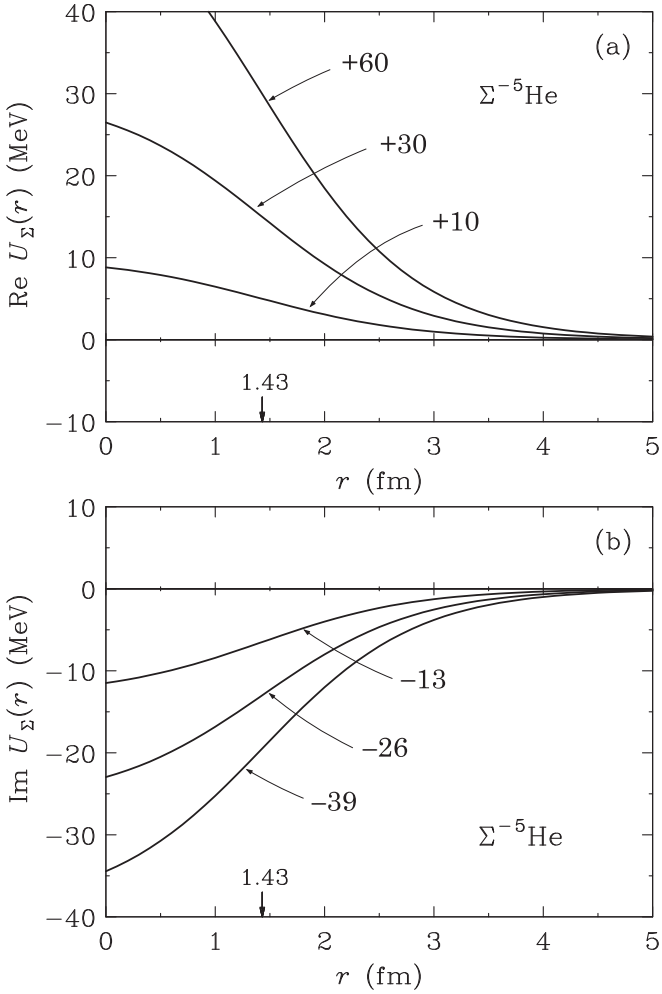

FIG. 5. (a) Real and (b) imaginary parts of the Σ-nucleus potentials U_Σ for Σ^--^{5}He. Solid curves denote the WS potential which has the strength of $V_\Sigma = +60, +30$, and $+10$ MeV and $W_\Sigma = -13, -26$, and -39 MeV with $R = r_0 A^{1/3} = 1.43$ fm where $r_0 = 0.835$ fm and $a = 0.706$ fm.

which reproduce the radial shape of the form factor very well, as seen in Fig. 4; the rms radius of the potential [34,39] denotes

$$\langle r^2 \rangle_U^{1/2} = \frac{\int r^2 U_\Sigma(r) d\boldsymbol{r}}{\int U_\Sigma(r) d\boldsymbol{r}} = 2.84 \text{ fm}. \quad (21)$$

A spin-orbit potential for Σ is also considered to denote a term of $V_{\rm so}^\Sigma (1/r)[df(r)/dr]\boldsymbol{\sigma}\cdot\boldsymbol{L}$, where $V_{\rm so}^\Sigma \simeq \frac{1}{2} V_{\rm so}^N \simeq 10$ MeV [40].

The strength parameters of (V_Σ, W_Σ) should be adjusted appropriately to reproduce available experimental data. A spreading imaginary potential W_Σ can represent complicated continuum states of ${}^6_\Lambda$H*. It should be noticed that the nuclear structure of ^{5}H$(1/2^+_{\rm g.s.})$ as the core nucleus is rather uncertain [41–43] although a resonant state at $E_{\rm ex} \simeq 1.7$ MeV has been identified in Ref. [44]. We assume that the ^{5}H core state with $\Gamma \simeq 2$ MeV is located at $E_{\rm ex} = 4.0$ MeV above the ^{3}H + 2n threshold, as suggested in Refs. [3,27]. Thus we have the Λ emitted threshold ($E_\Lambda = 0$ MeV) corresponding to the ${}^4_\Lambda$H$(1^+_{\rm exc.}) + 2n$ threshold at $M_{\rm x} = 5802.79$ MeV/c^2, so that

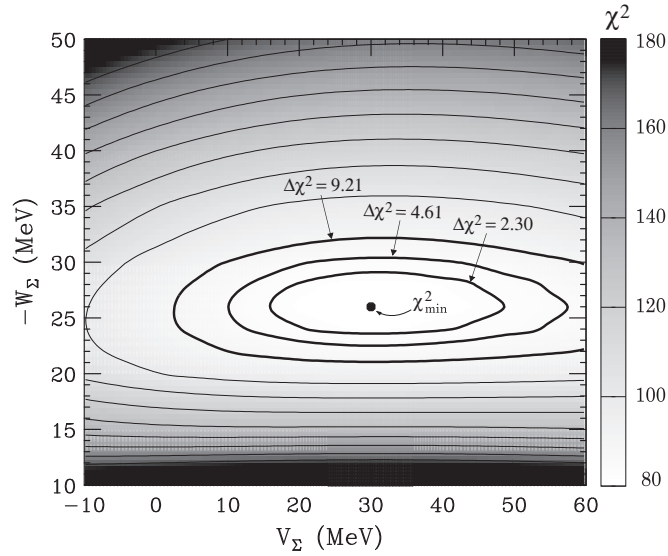

FIG. 6. Contour plots of the χ^2-value distribution in the $\{V_\Sigma, -W_\Sigma\}$ plane from fitting to the average cross section of $\bar{\sigma}_{2^\circ\text{-}14^\circ}$ in the ^{6}Li(π^-, K^+) reaction at $p_{\pi^-} = 1.2$ GeV/c. A solid circle denotes the minimum position of $\chi^2_{\rm min} = 84.5$ at $(V_\Sigma, -W_\Sigma) = (30$ MeV, 26 MeV) with $f_s = 1.23$. Thick curves indicate $\Delta\chi^2 = 2.30$, 4.61, and 9.21 which correspond to 68%, 90%, and 99% confidence levels for two parameters, respectively.

the threshold-energy difference between Σ^--^{5}He and Λ-^{5}H channels becomes $\Delta M = M(^5\text{He}) + m_{\Sigma^-} - M(^5\text{H}) - m_\Lambda = 56.9$ MeV.

Consequently, we attempt to determine the values of (V_Σ, W_Σ) phenomenologically by fitting to the shape and magnitude of the continuum spectra in Λ and Σ regions from the data of the J-PARC E10 experiment. In Fig. 5, we show the real and imaginary parts of the Σ-nucleus potentials for

TABLE I. The χ^2 fitting for various strength parameters, V_Σ and W_Σ, in the WS potential for Σ^--^{5}He, where $r_0 = 0.835$ fm and $a = 0.706$ fm. The value of χ^2/N and the renormalization factor f_s are obtained by comparing the calculated spectrum with the $N = 66$ data points of the average cross sections of $\bar{\sigma}_{2^\circ\text{-}14^\circ}$ for the missing mass $M_{\rm x} = 5790$–5920 MeV/c^2. The data were taken from Ref. [2].

V_Σ	W_Σ	$\bar{\sigma}_{2^\circ\text{-}14^\circ}$	
(MeV)	(MeV)	χ^2/N	f_s
−10	−13	159.8/66	1.00
0	−13	160.1/66	1.11
+30	−13	162.9/66	1.51
+60	−13	159.3/66	1.93
−10	−26	104.9/66	0.85
0	−26	95.5/66	0.94
+30	−26	84.5/66	1.23
+60	−26	89.8/66	1.53
−10	−39	141.4/66	0.74
0	−39	130.3/66	0.81
+30	−39	115.8/66	1.03
+60	−39	121.6/66	1.26

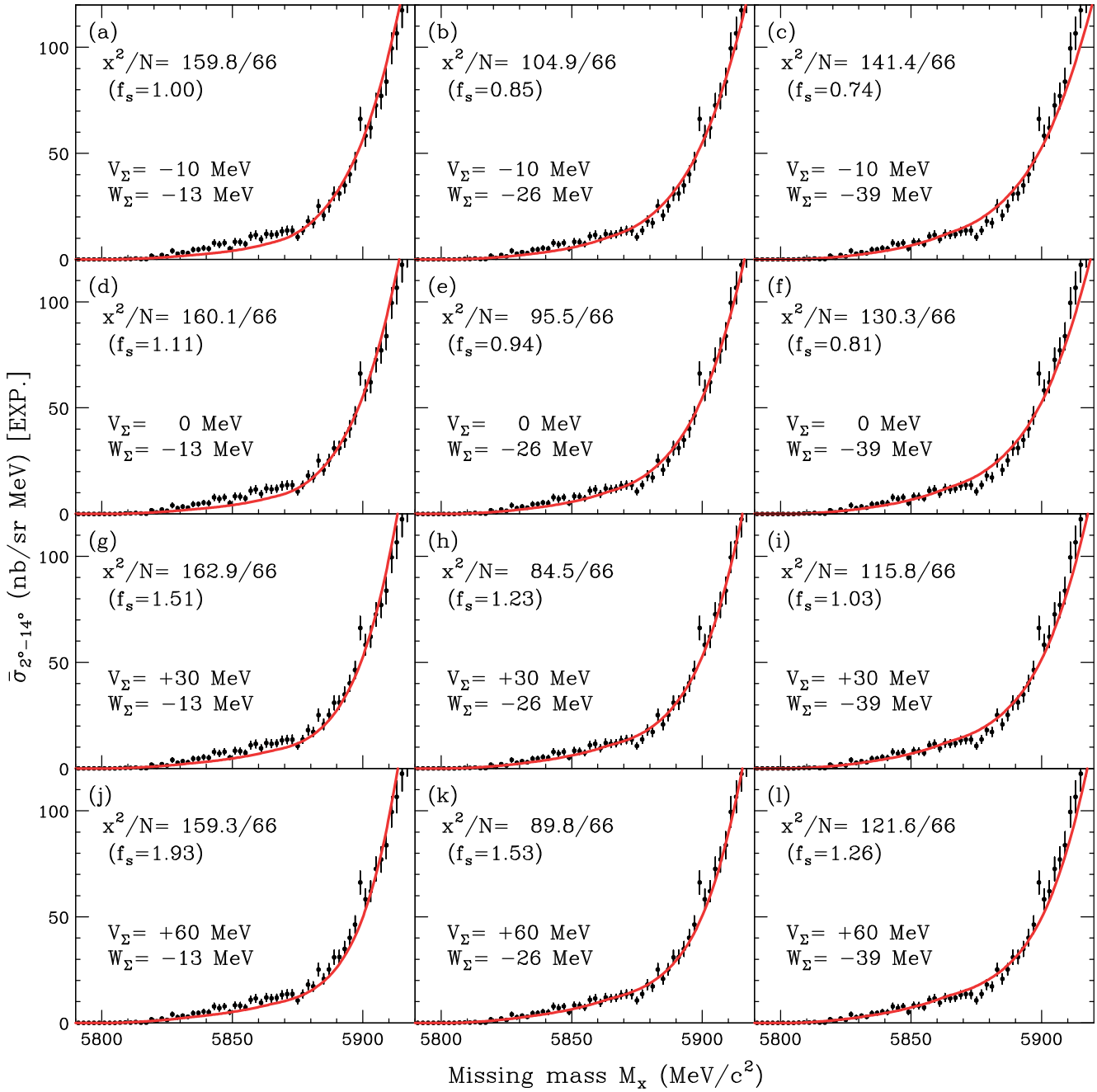

FIG. 7. Comparison of the calculated spectra for $\bar{\sigma}_{2^\circ\text{-}14^\circ}$ with the data of the ^{6}Li(π^-, K^+) reaction at $p_{\pi^-} = 1.2$ GeV/c [2]. Solid curves denote the spectrum for the WS potential with (V_Σ, W_Σ) listed in Table I, together with the value of χ^2/N and the renormalization factor f_s. The spectra are folded with a detector resolution of 3 MeV FWHM.

Σ^--^{5}He, choosing the best-fit strengths of $V_\Sigma = +30$ MeV and $W_\Sigma = -26$ MeV to fully explain the data of the ^{6}Li(π^-, K^+) data, as we will discuss them in the following sections.

V. RESULTS

Now we calculate the inclusive K^+ spectra for Σ^--^{5}He ($^6_\Sigma$H; $T = 3/2$) using the Green's function method [21] in order to be compared with the data of the ^{6}Li(π^-, K^+) reaction at the incident π^- momentum of $p_{\pi^-} = 1.2$ GeV/c and the K^+ forward-direction angles of $\theta_{\rm lab} = 2^\circ$–$14^\circ$. The average cross section $\bar{\sigma}_{2^\circ\text{-}14^\circ}$ is given by

$$\bar{\sigma}_{2^\circ\text{-}14^\circ} \equiv \int_{\theta_{\rm lab}=2^\circ}^{\theta_{\rm lab}=14^\circ} \left(\frac{d^2\sigma}{dEd\Omega}\right) d\Omega \Big/ \int_{\theta_{\rm lab}=2^\circ}^{\theta_{\rm lab}=14^\circ} d\Omega \qquad (22)$$

in the laboratory frame. To make a fit to the spectral shape of the data, we will introduce a renormalization factor of f_s into the absolute value of the calculated spectrum because the amplitude of $\overline{f}_{\pi^- p \to K^+ \Sigma^-}$ would have some ambiguities.

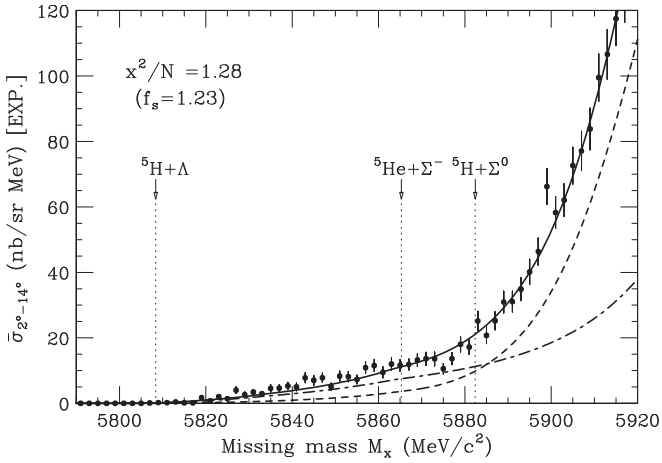

FIG. 8. Calculated spectrum for $\bar{\sigma}_{2^\circ\text{-}14^\circ}$ in the WS potential with $V_\Sigma = +30$ MeV, $W_\Sigma = -26$ MeV, $r_0 = 0.835$ fm, and $a = 0.706$ fm, together with the data of the ^{6}Li(π^-, K^+) reaction at $p_{\pi^-} = 1.2$ GeV/c [2]. Solid, dot-dashed, and dashed curves denote total, s-hole, and p-hole contributions, respectively. The spectra are folded with a detector resolution of 3 MeV FWHM.

A. Average cross section

1. χ^2 fitting

We examine the dependence of the spectral shape on two important strength parameters of (V_Σ, W_Σ) in the WS potential with $R = r_0 A_{\text{core}}^{1/3} = 1.428$ fm and $a = 0.706$ fm, comparing the calculated spectrum for $\bar{\sigma}_{2^\circ\text{-}14^\circ}$ with the data of the ^{6}Li(π^-, K^+) reaction at 1.2 GeV/c from the J-PARC E10 experiment [2]. We obtain the values of χ^2 for fits to the data points of $N = 66$ in the missing mass $M_x = 5790$–5920 MeV/c^2, varying the strengths of (V_Σ, W_Σ) and f_s; we estimate the average cross section in Eq. (22), calculating the spectra for $\theta_{\text{lab}} = 2^\circ$–$14^\circ$ in parameter region of $V_\Sigma = (-20)$–$(+80)$ MeV and $-W_\Sigma = 0$–60 MeV by a 5 MeV energy step. The 2 MeV energy step is taken in the estimation near the χ^2_{min} point.

Figure 6 displays the contour plots of χ^2-value distribution for $\bar{\sigma}_{2^\circ\text{-}14^\circ}$. The minimum value of χ^2 is found to be $\chi^2_{\text{min}} = 84.5$ at $V_\Sigma = +30$ MeV, $W_\Sigma = -26$ MeV, and $f_s = 1.23$, leading to elliptic regions of $\Delta\chi^2 = 2.30, 4.61$, and 9.21, which correspond to 68%, 90%, and 99% confidence levels for two parameters, respectively, where $\Delta\chi^2 \equiv \chi^2 - \chi^2_{\text{min}}$. Therefore, Fig. 6 clearly shows that a repulsive potential for Σ^--^{5}He is needed to reproduce the data. In Table I, we show the reduced χ^2 values of χ^2/N in calculations when $V_\Sigma = -10$, 0, $+30$, and $+60$ MeV and $W_\Sigma = -13$, -26, and -39 MeV, comparing the calculated spectra with the data, as shown in Fig. 7. We find that the value of χ^2/N is fairly changed by W_Σ and it is also dependent on V_Σ although the visible difference of the fitting in Fig. 7 does not seem to be so clear. This analysis indicates that the shape and magnitude of the calculated spectrum are sensitive to (V_Σ, W_Σ); the calculated spectrum for $(V_\Sigma, W_\Sigma) \simeq (+30$ MeV, -26 MeV$)$ is in good agreement with that of the data because it gives the minimum value of $\chi^2/N = 84.5/66 = 1.28$.

In Fig. 8, we show the absolute values of the calculated spectrum for $\bar{\sigma}_{2^\circ\text{-}14^\circ}$ with $(V_\Sigma, W_\Sigma) = (+30$ MeV, -26 MeV$)$ in comparison with the data for $M_x = 5790$–5920 MeV/c^2. We find the contribution of p-hole configurations is larger than that of s-hole configurations in the Σ continuum region; the latter configurations dominate in the Λ continuum region below the ^{5}He$+\Sigma^-$ threshold, where the production strength mainly arises from a term of $G_\Sigma^\dagger(\text{Im}U_\Sigma)G_\Sigma$ describing the $\Sigma^- p \to \Lambda n$ processes in ^{5}He together with the core-nucleus breakup [14]. The optimal Fermi averaging for the $\pi^- p \to K^+\Sigma^-$ reaction also indicates a good description of the energy in the Λ and Σ^- QF spectra in the nuclear (π^-, K^+) reaction.

2. Repulsion and absorption

To see effects of the repulsion and absorption in the Σ^--^{5}He potential, we discuss the shapes and magnitudes of the calculated spectra depending on the strengths of V_Σ and W_Σ. Figure 9 shows the absolute values of the calculated

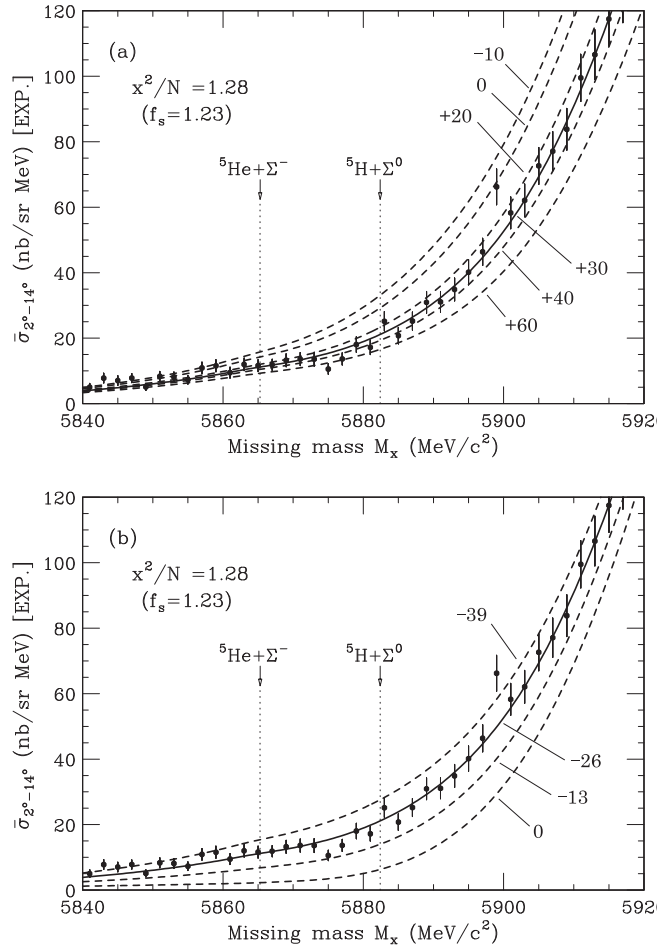

FIG. 9. Shapes and magnitudes of the calculated spectra for $\bar{\sigma}_{2^\circ\text{-}14^\circ}$ in the ^{6}Li(π^-, K^+) reaction at $p_{\pi^-} = 1.2$ GeV/c, depending on (a) the strengths of V_Σ when $W_\Sigma = -26$ MeV is chosen and (b) the strengths of W_Σ when $V_\Sigma = +30$ MeV is chosen. Solid curves denote the spectrum for the WS potential with $(V_\Sigma, W_\Sigma) = (+30$ MeV, -26 MeV$)$ as a guide. The spectra are folded with a detector resolution of 3 MeV FWHM.

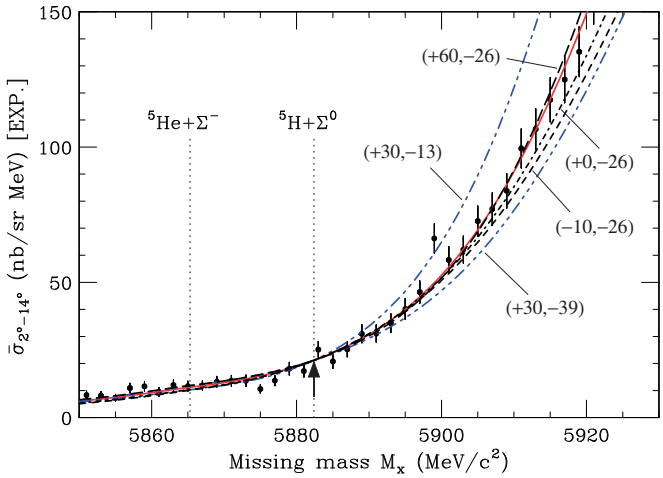

FIG. 10. Comparison among the shapes of the calculated spectra for $\bar{\sigma}_{2°\text{-}14°}$ in the ^{6}Li(π^-,K^+) reaction at $p_{\pi^-} = 1.2$ GeV/c, together with the data [2]. The solid curve denotes the spectrum with $(V_\Sigma, W_\Sigma) = (+30$ MeV, -26 MeV) and $f_s = 1.23$ as a guide. All the spectra for (V_Σ, W_Σ) are renormalized at the point of the arrow corresponding to the Σ^0 threshold ($M_x = 5882.4$ MeV/c^2) to be compared among the shapes of them. The spectra are folded with a detector resolution of 3 MeV FWHM.

spectra for $\bar{\sigma}_{2°\text{-}14°}$, using various strengths of V_Σ and W_Σ around the Σ threshold. As seen in Fig. 9(a), the magnitude of the spectra in the Σ^- region decreases and its slope becomes larger as the repulsion increases. When the absorption increases, the yields in the Λ region grow up, as shown in Fig. 9(b); the shape of the spectra trends to become flat, as a function of M_x. To clearly see a change of the shape of the spectrum on the parameter set, we display the calculated spectra for (V_Σ, W_Σ), renormalizing them for fits to the spectrum with $(V_\Sigma, W_\Sigma) = (+30$ MeV, -26 MeV) at the Σ^0 threshold ($M_x = 5882.4$ MeV/c^2), as shown in Fig. 10. We find that the slope of the spectrum in the Σ^- region is fairly enlarged, as a function of M_x, when the repulsion increases and the absorption decreases. We recognize that the shape of the spectrum is significantly changed by the repulsion and absorption in the WS potential. Therefore, we confirm that the Σ^--^{5}He potential has a repulsion in the real part and a sizable absorption in the imaginary part; the strengths denote

$$\begin{aligned} V_\Sigma &= +30 \pm 10 \text{ MeV}, \\ W_\Sigma &= -26 \pm 2 \text{ MeV}, \end{aligned} \tag{23}$$

in the WS potential with $r_0 = 0.835$ fm and $a = 0.706$ fm, as seen in Fig. 6. This potential provides the ability to explain the ^{6}Li(π^-, K^+) data at the J-PARC E10 experiment, although the radial shape of the WS potentials containing pure repulsion never explain the Σ^- atomic data [10,11].

B. Angular distributions

Figure 11 displays the angular distributions for the calculated spectra with $(V_\Sigma, W_\Sigma) = (+30$ MeV, -26 MeV) at $\theta_{\rm lab} = 3°$, 5°, 7°, 9°, 11°, and 13° for the missing mass $M_x =$ 5790–5920 MeV/c^2 at 1.2 GeV/c. In Table II, we show the results of the values of χ^2 for fits to the data of the angular distributions of $\theta_{\rm lab} = 2°$–14° [2]. We confirm that the shapes and magnitudes of the calculated spectra with $V_\Sigma = +30 \pm 10$ MeV and $W_\Sigma = -26 \pm 2$ MeV are almost consistent with those of the data, i.e., $\chi^2_{\rm tot}/N_{\rm tot} = 459.6/396 = 1.16$ where $N_{\rm tot} = 66 \times 6 = 396$, and a renormalization factor $f_s = 1.19$ depending on the absolute values of $\overline{f}_{\pi^- p \to K^+ \Sigma^-}$. However, we find that it is difficult to determine the parameters of (V_Σ, W_Σ) by only fits to each datum of the angular distribution at $\theta_{\rm lab} =$ 9°, 11°, and 13° because the χ^2 values are slightly sensitive to the parameters within the experimental errors; the data of the forward angles of $\theta_{\rm lab} \leqslant 8°$ are important to determine the parameters of the potential.

VI. DISCUSSION

A. Potential strengths

To see the validity of the Σ^--^{5}He potential given in Eq. (23), we consider the dependence of $A_{\rm core}$ on potential parameters in the Σ-nucleus potential. The folding model shows that the strength in Eq. (13) is written as

$$V_\Sigma + i W_\Sigma = [\bar{v}_{\Sigma N} + i \bar{w}_{\Sigma N} g(E_\Lambda)](\sqrt{\pi} a_{\Sigma N})^3 F(0), \tag{24}$$

where $F(0)$ is the form factor at the nuclear center in Eq. (18). When we use the strengths of (V_Σ, W_Σ) in Eq. (23), $a_{\Sigma N} =$ 1.2 fm, and $F(0) = 0.103$ fm^{-3} for $A_{\rm core} = 5$, we find

$$\begin{aligned} \bar{v}_{\Sigma N} &= +30 \pm 10 \text{ MeV}, \\ \bar{w}_{\Sigma N} &= -26 \pm 2 \text{ MeV}. \end{aligned} \tag{25}$$

Using Eq. (25) in the folding model, we obtain the Σ^--^{27}Al potential in which the strengths of

$$\begin{aligned} V_\Sigma &= +37 \pm 12 \text{ MeV}, \\ W_\Sigma &= -32 \pm 3 \text{ MeV}, \end{aligned} \tag{26}$$

are determined with the WS form having $R = 1.1 A_{\rm core}^{1/3}$, $a =$ 0.67 fm, and $F(0) = 0.127$ fm^{-3} for $A_{\rm core} = 27$. We find that the strength of V_Σ in Eq. (26) is slightly larger than that of $V_\Sigma =$ (+20)–(+30) MeV for Σ^--^{27}Al [10], whereas the strength of W_Σ in Eq. (26) is as large as that of $W_\Sigma = (-20)$–(-40) MeV for Σ^--^{27}Al [10]. We believe that the repulsive and absorptive components of the Σ^--^{5}He potential are consistent with those of the Σ^--^{27}Al potential quantitatively. If we extend the folding model to the nuclear matter (n.m.), we obtain the s.p. potential as

$$\begin{aligned} U_\Sigma(\text{n.m.}) &= \int v_{\Sigma N}(\boldsymbol{r} - \boldsymbol{r}') \sum_{|k| < k_F, s, t} \left| \frac{1}{(2\pi)^{\frac{3}{2}}} e^{i \boldsymbol{k} \boldsymbol{r}'} \eta_s \eta_t \right|^2 d\boldsymbol{r}' \\ &= (\bar{v}_{\Sigma N} + i \bar{w}_{\Sigma N})(\sqrt{\pi} a_{\Sigma N})^3 \frac{2 k_F^3}{3\pi^2}, \end{aligned} \tag{27}$$

where η_s (η_t) is a spin (isospin) function for a nucleon, and k_F is the Fermi momentum of 1.36 fm^{-1}. Using Eq. (25), we find

$$\begin{aligned} \text{Re } U_\Sigma(\text{n.m.}) &= +48 \pm 16 \text{ MeV}, \\ \text{Im } U_\Sigma(\text{n.m.}) &= -42 \pm 3 \text{ MeV}, \end{aligned} \tag{28}$$

which should be regarded as the depths of the Σ^- s.p. potential in nuclear matter of $(N - Z)/(N + Z) = 0.2$ at the normal density. Therefore, we show that the Σ^--^{5}He potential has

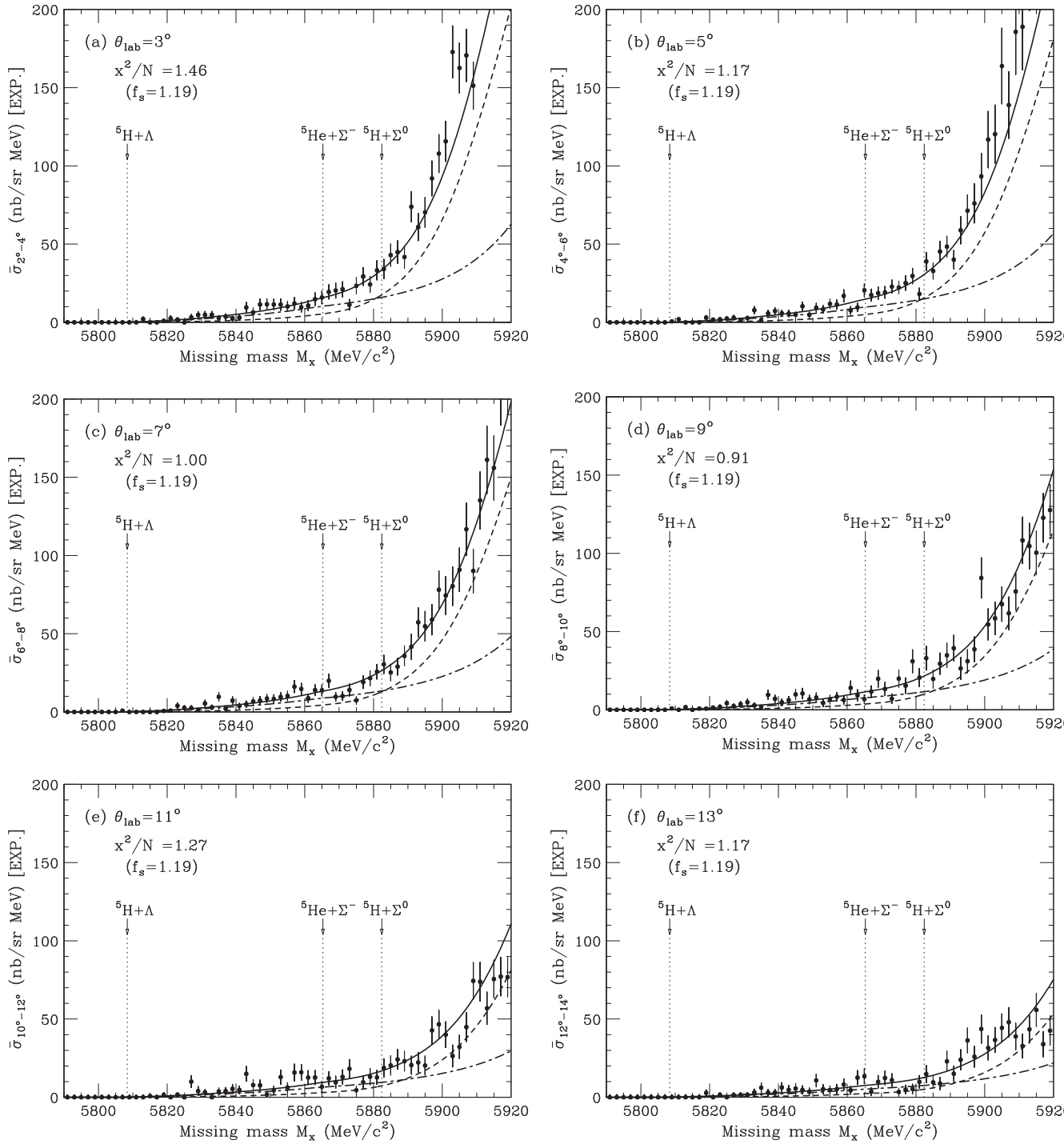

FIG. 11. Calculated spectra of the ^{6}Li(π^-, K^+) reaction at $p_{\pi^-} = 1.2$ GeV/c and K^+ forward-direction angles of (a) $\theta_{lab} = 3°$, (b) 5°, (c) 7°, (d) 9°, (e) 11°, and (f) 13°, as a function of the missing mass M_x. The strengths of $(V_\Sigma, W_\Sigma) = (+30$ MeV, -26 MeV) are used in the WS potential with $r_0 = 0.835$ fm and $a = 0.706$ fm. Solid, dot-dashed, and dashed curves denote total, s-hole, and p-hole contributions, respectively, where the calculated spectra are normalized by a common factor $f_s = 1.19$. The spectra are folded with a detector resolution of 3 MeV FWHM. The data are taken from Ref. [2].

the repulsion in the real part with the sizable imaginary part involving uncertainty within the experimental errors, consistent with the results in the previous works [10,11].

B. Volume integral

To evaluate the repulsion and absorption in the potentials, we show a volume integral per nucleon of the potential [10],

TABLE II. The χ^2 fitting for various strength parameters, V_Σ and W_Σ, in the WS potential for Σ^--^{5}He, where $r_0 = 0.835$ fm and $a = 0.706$ fm. The value of χ^2 and the common renormalization factor f_s are obtained by comparing the calculated spectrum with the $N = 66$ data points of the angular distributions at $\theta_{\rm lab} = 3^\circ$, 5°, 7°, 9°, 11°, and 13° for the missing mass $M_{\rm x} = 5790$–5920 MeV/c^2. The data were taken from Ref. [2].

V_Σ	W_Σ	χ^2						$\chi^2_{\rm tot}$ [a]	f_s
(MeV)	(MeV)	2°–4°	4°–6°	6°–8°	8°–10°	10°–12°	12°–14°		
−10	−13	88.4	87.3	74.9	83.7	106.8	87.3	492.3	0.97
0	−13	78.0	83.2	70.5	85.9	107.8	88.2	496.8	1.08
+30	−13	67.2	77.4	65.9	88.6	105.8	88.4	618.5	1.47
+60	−13	70.3	76.6	64.9	85.1	99.3	84.8	478.6	1.89
−10	−26	136.2	92.6	82.1	61.4	85.5	75.4	469.7	0.82
0	−26	120.8	86.1	75.2	60.7	85.4	75.9	590.4	0.91
+30	−26	96.6	77.2	65.7	60.1	83.7	77.0	459.6	1.19
+60	−26	94.5	79.2	66.6	60.2	81.1	77.3	428.9	1.50
−10	−39	210.5	124.2	111.2	64.4	79.3	74.2	545.3	0.71
0	−39	194.8	118.1	104.7	62.6	78.9	74.6	448.4	0.78
+30	−39	167.0	109.2	94.4	60.6	77.7	76.2	427.6	0.99
+60	−39	160.6	110.6	94.3	61.6	77.0	78.0	542.5	1.23

[a] $\chi^2_{\rm tot} = \sum \chi^2$ for all data points of $N_{\rm tot} = 66 \times 6 = 396$.

which is defined by

$$J_R + i J_I = \frac{1}{A_{\rm core}} \int U_\Sigma(r) d\boldsymbol{r}. \tag{29}$$

For the Σ^--^{5}He potential, we obtain

$$(J_R, J_I) \simeq (257\ \text{MeV fm}^3,\ -222\ \text{MeV fm}^3), \tag{30}$$

using $(V_\Sigma, W_\Sigma) = (+30\ \text{MeV}, -26\ \text{MeV})$ with $r_0 = 0.835$ fm and $a = 0.706$ fm, in comparison with $(J_R, J_I) \simeq (236\ \text{MeV fm}^3, -314\ \text{MeV fm}^3)$ for the Σ^--^{27}Al potential with $(V_\Sigma, W_\Sigma) = (+30\ \text{MeV}, -40\ \text{MeV})$. We find that the value of J_R for Σ^--^{5}He is almost similar to that for Σ^--^{27}Al, rather than the value of J_I. The value of J_I for Σ^--^{5}He is as large as that for Σ^--^{27}Al by a factor of 0.7. This seems to originate from the nuclear structure of the $\alpha + n$ cluster or the unsaturation density for ^{5}He because the volume integral is fairy affected by a k_F dependence of the effective ΣN interaction in the nucleus. To clearly understand the repulsion and absorption in the potential, we need more theoretical investigations based on microscopic description.

C. Size and potential range

The size and shape of the folding-model potential depends on the range of the two-body force. Here we discuss the parameters of (r_0, a) in the Σ^--^{5}He potentials adjusted to give a best least-squares fit to the radial shape of the form factors obtained by folding several ranges of the ΣN force into the matter MHO density distribution, following the procedure in Sec. IV. Considering $a_{\Sigma N} = 0.8$, 1.2, and 1.6 fm as a Gaussian range in Eq. (17), we obtain the WS potentials with the adjusted parameters of (r_0, a), and show the corresponding values of χ^2 for the best fit to the data of $\bar{\sigma}_{2^\circ\text{-}14^\circ}$ in Table III; the value of $\chi^2_{\rm min} = 84.5$ when $a_{\Sigma N} = 1.2$ fm is minimum in comparison with $\chi^2_{\rm min} = 84.7$ (86.1) when $a_{\Sigma N} = 0.8$ (1.6) fm. We repeat that for $a_{\Sigma N} = 1.2$ fm the strengths of $(V_\Sigma, W_\Sigma) = (+30\ \text{MeV}, -26\ \text{MeV})$ are favored for fits to the data, using the WS potential with $r_0 = 0.835$ fm and $a = 0.706$ fm, as already shown in Table I. We stress that the potential parameters for Σ^--^{5}He should be carefully adopted due to the unsaturation properties of the light nuclear core, as discussed in Sec. IV A.

On the other hand, the calculated spectra are rather insensitive to the potential with the parameters of (r_0, a) that give the similar values of $J_R + i J_I$ with the best-fit (V_Σ, W_Σ). In a previous work for Σ^--^{5}He [3], we used the WS potential with $r_0 = 1.1$ fm and $a = 0.67$ fm, of which parameters were used in the analysis of the (π^-, K^+) reactions on the heavier targets [3]. We obtained $\chi^2_{\rm min} = 87.6$ when the best fit $(V_\Sigma, W_\Sigma) = (+20\ \text{MeV}, -20\ \text{MeV})$. Because the value of $r_0 = 1.1$ fm seems to be too large for $A_{\rm core} = 5$, the Σ^--^{5}He potential should be improved by $(V_\Sigma, W_\Sigma) = (+30\ \text{MeV}, -26\ \text{MeV})$ with $r_0 = 0.835$ fm and $a = 0.706$ fm, as shown in Fig. 5. Nevertheless, one expects that the Σ^- wave functions related to the contribution of $\Sigma\Lambda$ couplings in ${}^{6}_{\Lambda}$H are not modified because the previous potential with $r_0 = 1.1$ fm and $a = 0.67$ fm gives the similar volume integral of Eq. (30), i.e., $(J_R, J_I) = (253\ \text{MeV fm}^3, -253\ \text{MeV fm}^3)$ for $(V_\Sigma, W_\Sigma) = (+20\ \text{MeV}, -20\ \text{MeV})$.

D. Angular dependence of Fermi-averaged amplitudes

In Table II, we showed the results of the values of χ^2 for fits to the data of the angular distributions at $\theta_{\rm lab} = 3^\circ$, 5°, 7°, 9°, 11°, and 13°. We realized that $V_\Sigma = +30 \pm 10$ MeV and $W_\Sigma = -26 \pm 2$ MeV are favored to reproduce the data of the angular distributions, so that $\chi^2_{\rm tot} = 459.6$ and a common factor $f_s = 1.19$ are determined. However, the angular distributions usually depend on the Fermi-averaged amplitudes of $\overline{f}_{\pi^- p \to K^+ \Sigma^-}$ at $\theta_{\rm lab}$ as well as properties of the Σ-nucleus potentials. Here we test the angular dependence of $\overline{f}_{\pi^- p \to K^+ \Sigma^-}$ by introducing the renormalization factors of $f_{s,\theta}$ at each angle $\theta_{\rm lab}$, rather than a common factor of f_s. In Table IV, we show the results of χ^2/N values for fits to the data at each $\theta_{\rm lab}$ when we take $(V_\Sigma, W_\Sigma) = (+30\ \text{MeV}, -26\ \text{MeV})$. We find

TABLE III. Effects of a Gaussian range $a_{\Sigma N}$ in the two-body ΣN force on the Σ^--^{5}He potential. The values of χ^2 are obtained by fits to the data of the average cross section for $\bar{\sigma}_{2^\circ\text{-}14^\circ}$. The data were taken from Ref. [2].

$a_{\Sigma N}$	r_0[a]	a[a]	R[a]	V_Σ	W_Σ	$J_R + iJ_I$[b]	$\langle r^2\rangle_U^{1/2}$[c]	$\bar{\sigma}_{2^\circ\text{-}14^\circ}$	
(fm)	(fm)	(fm)	(fm)	(MeV)	(MeV)	(MeV)	(fm)	χ^2	f_s
0.8	0.701	0.646	1.20	+40	−35	$+231 + i(-202)$	6.56	84.7	1.235
1.2	0.835	0.706	1.43	+30	−26	$+257 + i(-222)$	8.06	84.5	1.227
1.6	0.997	0.778	1.71	+25	−20	$+324 + i(-259)$	10.1	86.1	1.168

[a]Parameters of the WS form: $f(r) = \{1 + \exp[(r - R)/a]\}^{-1}$, where $R = r_0 A_{\text{core}}^{1/3}$.
[b]$J_R + iJ_I = \int U(r)d\boldsymbol{r}/A_{\text{core}}$.
[c]$\langle r^2\rangle_U^{1/2} = \int r^2 U(r)d\boldsymbol{r}/\int U(r)d\boldsymbol{r}$.

$\chi^2_{\text{tot}}/N_{\text{tot}} = 388.5/396 = 0.981$, which is significantly improved by each $f_{s,\theta}$ in comparison with $\chi^2_{\text{tot}}/N_{\text{tot}} = 459.6/396 = 1.16$, as seen in Table II; the absolute values of $\overline{f}_{\pi^- p\to K^+\Sigma^-}$ at $\theta_{\text{lab}} = 3^\circ$ and 5° are enlarged by 13% and 7%, respectively, whereas those at $\theta_{\text{lab}} = 7^\circ$, 9°, 11°, and 13° are reduced by 10%, 6%, 8%, and 16%, respectively. This improvement may suggest that the angular distributions of the optimal Fermi-averaged amplitudes of $\overline{f}_{\pi^- p\to K^+\Sigma^-}$ still have some ambiguities, as well as the simplicity of the s.p. shell-model description for ^{6}Li and ^{5}He in our DWIA calculations.

E. Neutron-excess environment

The neutron-rich nuclei give us new information on properties of the nuclear structure and two-body NN force because of unusual behaviors of the excess neutrons such as neutron skin and neutron halo. The sizes of the neutron-rich He and Li isotopes are also discussed experimentally and theoretically [35]. The study of neutron-rich Σ hypernuclei is one of the most promising subjects to examine the hypernuclear potentials in the neutron-excess environment. In this work, the DCX reaction (π^-, K^+) on the ^{6}Li$(1^+; T = 0)$ target provides a population of the neutron-rich Σ^--^{5}He and Λ-^{5}H hypernuclei with $T = 3/2$, where effects of the potential strengths on the neutron-excess environments of $(N - Z)/(N + Z) = 0.2$–0.6 are expected to be enhanced.

Our analyses for the Σ^--^{5}He potential suggest the strength of Re $U_\Sigma \simeq +48 \pm 16$ MeV extrapolated to neutron-excess matter at the normal density, which is larger than that of Re $U_\Sigma \simeq (+20)$–$(+30)$ MeV obtained by usual $N \simeq Z$ nuclei. We show that the Σ^--^{5}He potential becomes more repulsive in the real part because the repulsion of $\Sigma N\ I = 3/2,\ ^3S_1$ increases in Σ^-+^{5}He with the neutron-excess environments of $(N - Z)/(N + Z) = 0.2$, and that it has a sizable absorption in the imaginary part because a conversion transition to continuum nuclear breakup states in $\Lambda + {}^5\text{H}^*$ with $(N - Z)/(N + Z) = 0.6$ would be enlarged.

However, it should be noticed that nuclear effects of the $\alpha + d$ cluster structure and the nuclear deformation in light nuclei, and the nuclear coupled channels in Λ-^{5}H continuum states [45] are not taken into account in our calculations. More theoretical investigations based on microscopic description are needed to clarify the nature of the Σ-nucleus potential.

VII. SUMMARY AND CONCLUSION

We have studied phenomenologically the inclusive spectra of the ^{6}Li(π^-, K^+) reaction at $p_{\pi^-} = 1.2$ GeV/c within the DWIA in order to clarify the property of the Σ-nucleus potential for Σ^--^{5}He. We have determined the strengths of (V_Σ, W_Σ) in the WS potential with $r_0 = 0.835$ fm and $a = 0.706$ fm by comparing the calculated continuum spectrum in Σ and Λ regions with the data of the J-PARC E10 experiment. We have also discussed effects of the size and potential range for Σ^--^{5}He in the neutron excess of $(N - Z)/(N + Z) = 0.2$. The results are summarized as follows:

(i) The calculated spectra with DWIA can fully reproduce the data of $\bar{\sigma}_{2^\circ\text{-}14^\circ}$ and the angular distribution at $\theta_{\text{lab}} = 2^\circ$–$14^\circ$ in the ^{6}Li(π^-, K^+) reaction at 1.2 GeV/c.
(ii) The repulsive and absorptive components for the Σ^--^{5}He potential indicate $V_\Sigma = +30 \pm 10$ MeV and $W_\Sigma = -26 \pm 4$ MeV in the WS potential so as to explain the data of the J-PARC E10 experiment.
(iii) The optimal Fermi-averaged amplitudes of $\overline{f}_{\pi^- p\to K^+\Sigma^-}$ in our DWIA calculations are essential

TABLE IV. The χ^2 values and the renormalization factors $f_{s,\theta}$ for each θ_{lab} by comparing the calculated spectrum with the $N = 66$ data points of the angular distributions for the missing mass $M_x = 5790$–5920 MeV/c^2. $V_\Sigma = +30$ MeV and $W_\Sigma = -26$ MeV are used in the WS potential. The value in the bracket is a ratio of $f_{s,\theta}$ to $f_s = 1.19$, which is taken as a common renormalization factor.

θ_{lab}	2°–4°	4°–6°	6°–8°	8°–10°	10°–12°	12°–14°	Total[a]
χ^2/N	68.6/66	70.6/66	65.3/66	56.1/66	65.3/66	62.7/66	388.5/396
$f_{s,\theta}$	1.35	1.28	1.17	1.12	1.01	1.00	
$(f_{s,\theta}/f_s)$	(1.13)	(1.07)	(0.90)	(0.94)	(0.92)	(0.84)	

[a]$\chi^2_{\text{tot}}/N_{\text{tot}}$ where $N_{\text{tot}} = 66 \times 6 = 396$.

to describe the energy and angular dependence of the data of the ^{6}Li(π^-, K^+) reaction at 1.2 GeV/c.

In conclusion, we show that the repulsive and absorptive components of the Σ^--^{5}He potential provide the ability to explain the data of the ^{6}Li(π^-, K^+) spectra at 1.2 GeV/c; the strengths of $V_\Sigma = +30 \pm 10$ MeV and $W_\Sigma = -26 \pm 2$ MeV are favored within the WS potential, consistent with analyses for heavier nuclei. We recognize that the calculated spectra via Σ^- doorways can reproduce the experimental data of the ^{6}Li(π^-, K^+) reaction at 1.2 GeV/c in Σ region as well as Λ region [3]. The detailed analysis based on microscopic calculations is required for the analyses of the J-PARC E10 experiment. This investigation is a subject for future research.

ACKNOWLEDGMENTS

The authors would like to thank Prof. A. Sakaguchi, Prof. H. Tamura, Dr. M. Ukai, and Prof. T. Fukuda for many valuable discussions. This work was supported by Grants-in-Aid for Scientific Research (KAKENHI) from the Japan Society for the Promotion of Science: Scientific Research on Innovative Areas (Grant No. JP24105008) and Scientific Research (C) (Grant No. JP25400278 and No. JP16K05363).

[1] H. Sugimura *et al.* (J-PARC E10 Collaboration), Phys. Lett. B **729**, 39 (2014).
[2] R. Honda *et al.* (J-PARC E10 Collaboration), Phys. Rev. C **96**, 014005 (2017).
[3] T. Harada and Y. Hirabayashi, Phys. Rev. C **95**, 044610 (2017).
[4] H. Noumi *et al.*, Phys. Rev. Lett. **89**, 072301 (2002); **90**, 049902(E) (2003).
[5] P. K. Saha *et al.*, Phys. Rev. C **70**, 044613 (2004).
[6] C. J. Batty, E. Friedman, and A. Gal, Phys. Lett. B **335**, 273 (1994); Prog. Theor. Phys. Suppl. **117**, 227 (1994).
[7] E. Friedman and A. Gal, Phys. Rep. **452**, 89 (2007).
[8] J. Mareš, E. Friedman, A. Gal, and B. K. Jennings, Nucl. Phys. A **594**, 311 (1995).
[9] J. Dabrowski, J. Rozynek, and G. S. Anagnostatos, Eur. Phys. J. A **14**, 125 (2002).
[10] T. Harada and Y. Hirabayashi, Nucl. Phys. A **759**, 143 (2005).
[11] T. Harada and Y. Hirabayashi, Nucl. Phys. A **767**, 206 (2006).
[12] C. B. Dover, D. J. Millener, and A. Gal, Phys. Rep. **184**, 1 (1989).
[13] T. Harada, Y. Akaishi, S. Shinmura, and H. Tanaka, Nucl. Phys. A **507**, 715 (1990).
[14] T. Harada, Phys. Rev. Lett. **81**, 5287 (1998); Nucl. Phys. A **672**, 181 (2000).
[15] M. Oka *et al.*, Phys. Lett. B **130**, 365 (1983).
[16] Th. A. Rijken *et al.*, Prog. Theor. Phys. Suppl. **185**, 14 (2010); Y. Fujiwara *et al.*, Prog. Part. Nucl. Phys. **58**, 439 (2007); H. Polinder *et al.*, Phys. Lett. B **653**, 29 (2007).
[17] S. R. Beane *et al.* (NPLQCD Collaboration), Phys. Rev. Lett. **106**, 162001 (2011); T. Inoue *et al.* (HAL QCD Collaboration), *ibid.* **106**, 162002 (2011).
[18] S. Balberg and A. Gal, Nucl. Phys. A **625**, 435 (1997); M. Baldo, G. F. Burgio, and H.-J. Schulze, Phys. Rev. C **58**, 3688 (1998); and references therein.
[19] A. Gal, E. V. Hungerford, and D. J. Millener, Rev. Mod. Phys. **88**, 035004 (2016).
[20] T. Inoue (HAL QCD Collaboration), PoS (**INPC2016**), 277 (2016).
[21] O. Morimatsu and K. Yazaki, Prog. Part. Nucl. Phys. **33**, 679 (1994); and references therein.
[22] J. Hüfner, S. Y. Lee, and H. A. Weidenmüller, Nucl. Phys. A **234**, 429 (1974).
[23] T. Harada and Y. Hirabayashi, Nucl. Phys. A **744**, 323 (2004).
[24] C B. Dover and A. Gal, Phys. Lett. B **110**, 433 (1982).
[25] Y. Fujiwara *et al.*, Prog. Theor. Phys. Suppl. **68**, 29 (1980); H. Furutani *et al.*, *ibid.* **68**, 193 (1980).
[26] A. Bohr and M. Mottelson, *Nuclear structure*, Vol. 1 (Benjamin, New York, 1969), p.238.
[27] D. R. Tilley *et al.*, Nucl. Phys. A **708**, 3 (2002).
[28] H. Tyeén *et al.*, Nucl. Phys. **79**, 321 (1966); G. Jacob and Th. A. J. Maris, Rev. Mod. Phys. **38**, 121 (1966); **45**, 6 (1973).
[29] H. de Vries, C. W. de Jager, and C. de Vries, At. Data Nucl. Tables **36**, 495 (1987).
[30] T. Harada, A. Umeya, and Y. Hirabayashi, Phys. Rev. C **79**, 014603 (2009).
[31] H. Kamano, S. X. Nakamura, T.-S. H. Lee, and T. Sato, Phys. Rev. C **88**, 035209 (2013).
[32] O. I. Dahl *et al.*, Phys. Rev. **163**, 1430 (1967); T. O. Binford *et al.*, *ibid.* **183**, 1134 (1969); W. Langbein and F. Wagner, Nucl. Phys. B **53**, 251 (1973); and references therein.
[33] S. A. Gurvitz, Phys. Rev. C **33**, 422 (1986).
[34] G. W. Greenlees, G. J. Pyle, and Y. C. Tang, Phys. Rev. **171**, 1115 (1968); G. W. Greenlees, W. Makofske, and G. J. Pyle, Phys. Rev. C **1**, 1145 (1970).
[35] I. Tanihata, H. Savajols, and R. Kanungod, Prog. Part. Nucl. Phys. **68**, 215 (2013).
[36] H. Überall, *Electron Scattering from Complex Nuclei, Part A* (Academic Press, New York, 1971), p. 197.
[37] Y. Sakuragi, M. Yahiro, and M. Kamimura, Prog. Theor. Phys. Suppl. **89**, 136 (1986); Prog. Theor. Phys. **70**, 1047 (1983).
[38] Y. Akaishi, T. Harada, S. Shinmura, and K. Swe Myint, Phys. Rev. Lett. **84**, 3539 (2000).
[39] S. Sakaguchi *et al.*, Phys. Rev. C **84**, 024604 (2011); **87**, 021601(R) (2013).
[40] O. Morimatsu, S. Ohta, K. Shimizu, and K. Yazaki, Nucl. Phys. A **420**, 573 (1984); Y. Fujiwara *et al.*, *ibid.* **674**, 493 (2000).
[41] A. Gal and D. J. Millener, Phys. Lett. B **725**, 445 (2013).
[42] E. Hiyama *et al.*, Nucl. Phys. A **908**, 29 (2013).
[43] A. H. Wuosmaa *et al.*, Phys. Rev. C **95**, 014310 (2017).
[44] A. A. Korsheninnikov *et al.*, Phys. Rev. Lett. **87**, 092501 (2001).
[45] T. Harada and Y. Hirabayashi, Nucl. Phys. A **934**, 8 (2015).